THREE-DIMENSIONAL BUBBLE-VELOCITY DETERMINATION ALGORITHM WITH WIRE-MESH SENSOR

T. KANAI[1, c], M. FURUYA[1], T. ARAI[1], K. SHIRAKAWA[1], Y. NISHI[1]

[1]Central Research Institute of Electric Power Industry, 2-11-1 Iwado-Kita, Komae, Tokyo 2018511, JAPAN

[c]Corresponding author: Tel.: +81334802111; Fax: +81334882844; Email: t-kanai@criepi.denken.or.jp

KEYWORDS:
Main subjects: flow visualization
Fluid: two-phase flow, air-water
Visualization method: wire mesh sensor
Other keywords: image processing, tracking, cross-correlation, bubble velocity

ABSTRACT:A gas-liquid two-phase flow in a large diameter pipe exhibits complex three-dimensional flow structures. A Wire-Mesh Sensor (WMS) consists of two parallel wire layers intersecting at right angles. Fig. 1 shows a schematic of the WMS used in this study. The WMS measures instantaneous two-dimensional void-fraction distribution on the pipe cross-section, according to the electric conductance between two intersecting wires in a two-phase flow. WMS can also acquire phasic velocity based on the time lag of void signals between two sets of WMS. Previously, the acquired phasic velocity was limited to one-dimensional. The authors propose an algorithm to estimate the three-dimensional bubble velocity according to each of the WMS measurement locations. The three-dimensional phasic velocity is determined by the tracking bubble. The proposed algorithm first identifies each bubble in the WMS signals, before subsequently seeking pairs of similar bubbles in two sets of WMS data according to bubble size and location. The validity of this method is demonstrated for a swirl flow and the proposed method can successfully visualize a swirl flow structure.

INTRODUCTION: Recent computing advances have enabled computational fluid dynamics (CFD) codes to predict two-phase flow in simple geometry. An accurate experimental database on a three-dimensional two-phase flow is crucial to validate such CFD codes. Extensive studies of the characteristics of two-phase flow have been used to address simple experimental correlations. Several measurement techniques have also been used successively to measure two-phase flow dynamics. Optical methods such as particle image velocimetry (PIV) and particle tracking velocimetry (PTV) based on high-speed camera images are non-intrusive, but only applicable for low void fractions. An ultrasonic velocity profile monitor (UVP)[(1)] and a void probe sensor[(2)] acquire information as one-point, while a quick closing valve method acquires information in time-averaged form. Therefore, it has been difficult to precisely determine the three-dimensional measurement of two-phase flow with these methods. To measure void fractions at high temporal and spatial resolutions, a wire-mesh sensor (WMS) has been proposed by Prasser et al.[(3)]. (1998). The WMS can acquire a local void fraction with principles based on local conductivity measurement and measure phasic velocity distribution by investigating the signal time-delay between two WMSs via cross-correlation analysis[(4-6)]. However, such phasic velocity measurement has been simply one-dimensional and axial, whereas the two-phase flow in a large diameter pipe shows three-dimensional complex behavior by nature, hence the importance of estimating the three-dimensional phasic velocity to improve the three-dimensional two-phase flow analysis codes. Furthermore, Prasser et al. proposed methods to investigate the flow evolution using WMS. The mechanism of bubble coalescence, break-up and lateral lift force was clarified by decomposing the void fraction according to the bubble size classification[(7-9)].

Previously, the acquired phasic velocity was limited to one-dimensional. The authors now propose an algorithm to estimate the three-dimensional bubble velocity according to each WMS measurement location. The three-dimensional phasic velocity is determined by the tracking bubble. The proposed algorithm first identifies each bubble in the WMS signals, before subsequently seeking pairs of similar bubbles in two sets of WMS data according to bubble size and location. The validity of this method is demonstrated for a swirl flow and the proposed method can successfully visualize a swirl flow structure.

EXPERIMENTALARRANGEMENTS: The WMS was developed at the Forschungszentrum Rossendorf (FzR, Germany) and consists of a pair of parallel wire layers located at the cross-section of a pipe. The parallel wires intersect at 90° with a small gap and each intersection acts as an electrode. The WMS allows the measurement of the instantaneous two-dimensional void-fraction distribution over the cross-section of a pipe, based on the difference between the local instantaneous conductivity of the two-phase flow. For a two-phase flow, the water phase shows slight conductance, while the gas phase acts as an insulator. During the signal acquisition, one plane of the electrode wires is used as a transmitter and the other as a receiver plane.

Fig. 1(a) shows a schematic view of the WMS used in this study. The inner diameter of the two sensors is 224 mm (equal to the test pipe). The WMS consists of 64 x 64 parallel wires, with both layers intersecting at 90º and a gap of 2.8 mm. The (horizontal) gap between the wires is 3.5 mm, which represents the horizontal spatial resolution of the sensor. Fig. 1 (b) shows a cross-sectional measurement signal of the two-phase flow. The diameter of the wires was 0.25 mm, with a negligible influence on the flow field and sufficient intensity. The distance between two layers of the sensor is 40 mm. The sampling frequency of such device can be set to a maximum of 1250 frames per second (fps). In this study, the sampling frequency is set to 1000 fps.

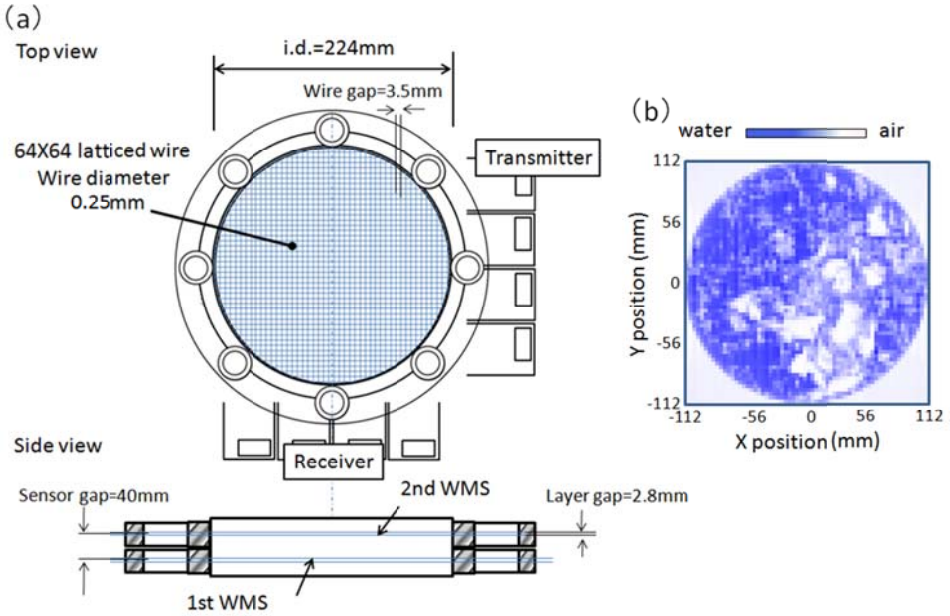

Fig. 1 (a) Schematics of WMS used in this study. The inner diameter of the two sensors is 224 mm (equal to the test pipe). The WMS consists of 64 x 64 parallel wires. The (horizontal) gap between the wires is 3.5 mm. The distance between two layers of the sensor is 40 mm. Fig. 1 (b) Cross-sectional measurement signal of the two-phase flow.

Fig. 2(a) shows a schematic view of the test facility, which mainly consists of a water circulation pump, air compressor, air receiver tank, air-water separation tank, heat exchanger and test pipe. The test section consists of a PVC pipe (i.d. 224 mm), while the total height of the facility is about 6 m. The straight run pipe upstream of the WMS is 20.3 D and downstream 3.7 D, where D (mm) is the inner diameter of the pipe. Fig. 2(c) shows a schematic view of the air injector. The test section has sixteen air-injection nozzles (i.d. 10 mm) on the circumference 14.3 D upstream of WMS. Fig. 2 (b) shows a schematic view of a Swirler, which consists of four vanes, an inner pipe (o.d. 110 mm) and an outer pipe (i.d. 220 mm). The Swirler is inserted 5.8 D upstream of WMS. The center angle of the vane was about 30 deg. and it was subject to counterclockwise rotation.

Experiments are performed in an air-water system. Water is passed through an ion-exchange resin and supplied to the test section via the lower plenum by the circulating water pump. Air is supplied to the test section through the air receiver tank with the air compressor and with the air receiver tank used to control the inlet pressure alteration. Downstream of the test section, air and water were separated at the separation tank, the separated air discharged into the atmosphere and the separated water recirculated into the water tank. The water temperature is maintained at 30 degrees Celsius by the heat exchanger. The water flow rate is measured by a magnetic flow meter (KEYENCE full-duplex-UH

100H) and controlled by regulating and bypass valves. The airflow was measured by 16 mass flow meters (Yamatake Co. Ltd., MCF015) and controlled by the air supply system. Table 1 shows the flow conditions and measurement setup of the WMS.

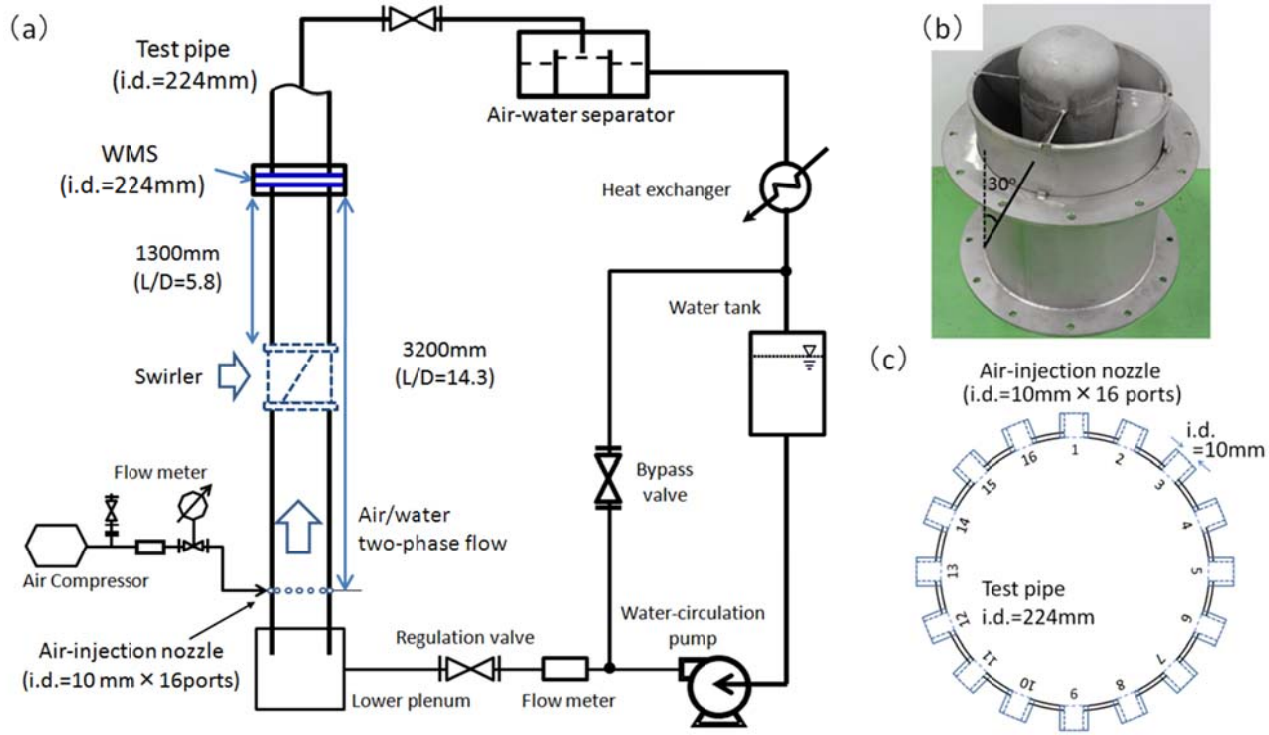

Fig. 2. The test section consists of a PVC pipe (i.d. 224 mm), with a total facility height of about 6 m. The straight run pipe upstream of the WMS is 20.3 D and the test section has sixteen air injectors (i.d. 10 mm) on the circumference 14.3 D upstream of WMS. (b): Photograph of the swirler, which comprises an outer pipe (i.d. 220 mm), inner pipe (o.d. 110 mm) and four vanes. (c): Schematic view of the air-injector nozzle.

Table 1. Experimental parameters and swirler

Inlet superficial liquid velocity; j_L(m/s)	0.63	
Inlet superficial phasic velocity; j_G(m/s)	Run 1	0.05
	Run 2	0.21
	Run 3	0.42
	Run 4	0.63
WMS sampling frequency (fps)	1000	
Measurement duration (s)	5 (5 cases per parameter)	
Ratio of Length to Diameter (L/D)		
Inlet Nozzle to WMS	14.3	
Swirler to WMS	5.8	
Swirler vane angle (°)	30, N/A (without generator)	

BUBBLE IDENTIFICATION: The two-phase flow data consist of a three-dimensional matrix 64 × 64 ×5000 ($i \times j \times k$). Each of these data contains two-dimensional void distributions of 64 × 64 WMS and 5000 time-series data. Bubble identification is via a special algorithm and a bubble is defined as a region of connected gas elements. The bubble volume is given by Eq. 1. The bubble volume can be obtained by summating the bubble elements, bubble velocity and the geometric structure of the WMS. Moreover, the bubble diameter is calculated by Eq. 2.

$$V_{\mathrm{B}}=U_{\mathrm{g}}\Delta x\Delta y\Delta t\sum_{i,j,k\in \mathrm{B}}\varepsilon_{\mathrm{i,j,k}} \tag{1}$$

$$D_{\mathrm{B}}=\sqrt[3]{\frac{6V_{\mathrm{B}}}{\pi}} \tag{2}$$

where V_{B} is the bubble volume, $\varepsilon_{\mathrm{i,j,k}}$ the void fraction at i, j, k, U_{g} the bubble velocity, Δx, Δy the wire gap (3.5 mm), and Δt the sampling period (1 msec) [8].

The coordinates of the center of mass can be obtained by averaging the measurement coordinates of all elements belonging to the selected bubble using the local void fraction values as a weight function (Eqs. 3-5). Fig. 3 shows an example of the bubble identification, with flow conditions of j_{G}= 0.21 m/s, j_{L}=0.63 m/s and a swirl flow. The bubble identification processes the bubble signal of about $V_{\mathrm{B}} \geq 300$ mm^3 ($D_{\mathrm{B}} \geq 8$ mm), since smaller bubbles ($D_{\mathrm{B}} < 8$ mm) seldom contribute to flow dynamics. Larger bubbles appear intermittently, as a result of x_{c} and y_{c} shows the bubbles wind through the test pipe.

$$x_{\mathrm{c}}=\frac{\sum_{i,j,k} j\cdot\Delta x\cdot\varepsilon_{i,j,k}}{\sum_{i,j,k}\varepsilon_{i,j,k}}, \tag{3}$$

$$y_{\mathrm{c}}=\frac{\sum_{i,j,k} i\cdot\Delta i\cdot\varepsilon_{i,j,k}}{\sum_{i,j,k}\varepsilon_{i,j,k}}, \tag{4}$$

$$t_{\mathrm{c}}=\frac{\sum_{i,j,k} k\cdot\Delta t\cdot\varepsilon_{i,j,k}}{\sum_{i,j,k}\varepsilon_{i,j,k}}, \tag{5}$$

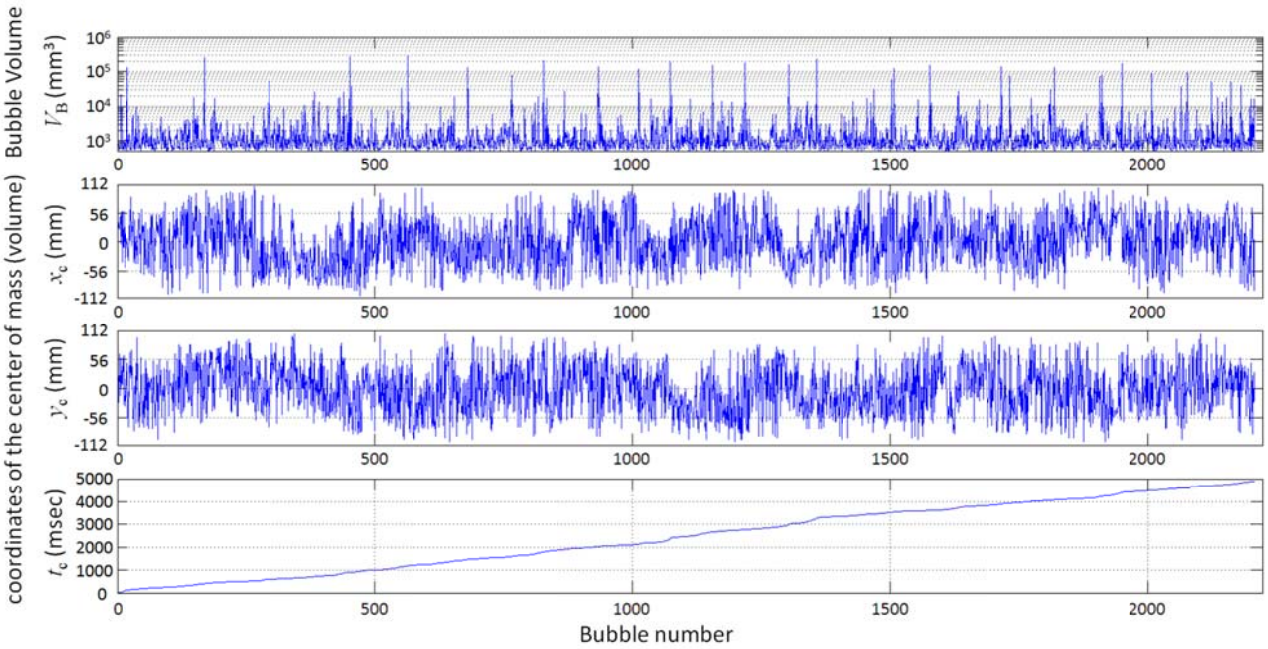

Fig. 3. An example of bubble identification. The flow conditions are j_{G}= 0.21 m/s, j_{L}=0.63 m/s and a swirl flow.

BUBBLE TRACKING: The three-dimensional phasic velocity is determined by tracking the bubble. Fig. 4 (left) shows the upstream and downstream WMS bubble identification results. The red and blue circles show bubbles measured by upstream and downstream WMS, respectively. The circle size and location refer to bubble size and location. Subsequently, pairs of similar bubbles are sought in two WMS data, according to bubble size and location. Table 2 shows matching conditions, tracking ranges and bubble classifications. The tracking ranges are as follows, with a time range (ΔT) of $10 \leq \Delta T \leq 200$. In the case of the swirl flow, the horizontal range (ΔX, ΔY) is $-10 \leq \Delta X_{WMS}, \Delta Y_{WMS} \leq 10$ at measurement points ($-35 \leq \Delta X, \Delta Y \leq 35$ in millimeter units). Conversely, in the case of the vertical upward flow, the horizontal range is $-7 \leq \Delta X_{WMS}, \Delta Y_{WMS} \leq 7$ in measurement points ($-24.5 \leq \Delta X, \Delta Y \leq 24.5$ in millimeter units). The conditions used to judge whether an identical element is present or not are $V_{B,1st}, V_{B,2nd} \geq 300$ mm^3 ($D_{B,1st}, D_{B,2nd} \geq 8$ mm) and several matching conditions (Volume Ratio: VR, shown in Table 2) in the tracking range. Fig. 4 (right) shows the result of matching ratio versus matching conditions (VR 1-5) at j_L=0.63 (m/s), j_G= 0.63 (m/s). In Fig. 5, bubbles are generally divided into four groups by bubble size, Group 1 is about $8 \leq D_B < 20$, Group 2 is about $20 \leq D_B < 30$, Group 3 is about $30 \leq D_B < 60$ and Group 4 is about $60 \leq D_B$. As the matching conditions become increasingly stringent, the matching ratio falls. Moreover, the matching ratio also declines in the large bubble group. Groups 3 and 4 show low matching ratios compared with Groups 1 and 2, since large bubbles generally have considerable deformation and few bubbles fulfill the condition.

The matching ratio is high with a loose matching condition, but the number of mistakes increases. Fig. 5 shows the result of bubble velocity distributions when the matching conditions (VR) are changed and the red solid lines show the gas-phasic velocity calculated via cross-correlation analysis by the bubble group. The results of VR4 and cross-correlation analysis concur. Moreover, small bubbles are generally slower than large bubbles. However, Run4-Gr1-Mc1 and Run4-Gr4-VR1 show fast and slow distributions, respectively. Run4-Gr1-VR4 shows slow distributions compared with Run4-Gr4-VR4. In this study, the matching condition of VR4 ($0.8 \leq V_{B,1st}/V_{B,2nd} \leq 1.2$) is adopted in the bubble tracking.

Moreover, the validity of this method is demonstrated for a swirl flow and a vertical upward flow. Fig. 7 shows the bubble velocity of the swirl flow, j_G= 0.21 m/s, j_L=0.63 m/s using bubble tracking. Fig. 7 (left) shows an overhead view, while Fig. 7 (right) shows a top view. The bubble tracking result effectively shows the swirl flow characteristics. Fig.8 shows comparisons of bubble tracking and cross-correlation analysis. The blue circles show bubble velocity estimated by bubble tracking, while the black lines show the averaged bubble velocities. Finally, the red line shows the velocity as estimated by cross-correlation analysis. Both results effectively match and demonstrate the efficacy of the bubble tracking method.

Table 2. Matching conditions, tracking range and bubble classifications

Matching condition (Volume Ratio: $V_{B,1st}/V_{B,2nd}$ (VR))	VR 1	0.33 (one third) $\leq VR \leq$ 3.0 (three times)
	VR 2	0.5 (half) $\leq VR \leq$ 2.0 (twice)
	VR 3	0.5(-50%) $\leq VR \leq$ 1.5 (+50%)
	VR 4	0.8(-20%) $\leq VR \leq$ 1.2 (+20%)
	VR 5	0.9(-10%) $\leq VR \leq$ 1.1 (+10%)
Tracking ranges (ΔX, ΔY)	Vertical upward flow	$-7 \leq \Delta X_{WMS}, \Delta Y_{WMS} \leq 7$ (points) $-24.5 \leq \Delta X, \Delta Y \leq 24.5$ (mm)
	Swirl flow	$-10 \leq \Delta X_{WMS}, \Delta Y_{WMS} \leq 10$ (points) $-35 \leq \Delta X, \Delta Y \leq 35$ (mm)
Tracking range (ΔT) (10^{-3}s)		$10 \leq \Delta T \leq 180$
Vertical velocity range ($u_{G,v}$) (m/s)		$0.22 \leq u_{G,h} \leq 4$
Bubble classifications		Bubble diameter (mm)
	Gr 1	$8 \leq D_B < 20$
	Gr 2	$20 \leq D_B < 30$
	Gr 3	$30 \leq D_B < 60$
	Gr 4	$60 \leq D_B$

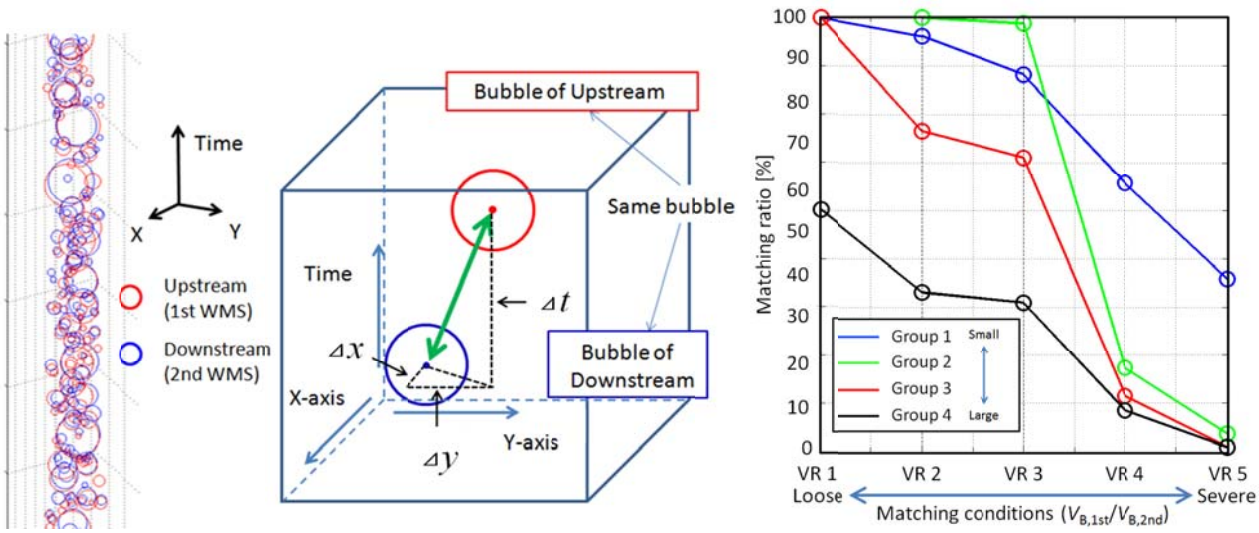

Fig. 4 (left). Principle of bubble tracking. Red and blue circles show bubbles measured by upstream and downstream WMS respectively. Fig. 4 (right). Matching ratio versus $V_{B,1st}/V_{B,2nd}$.

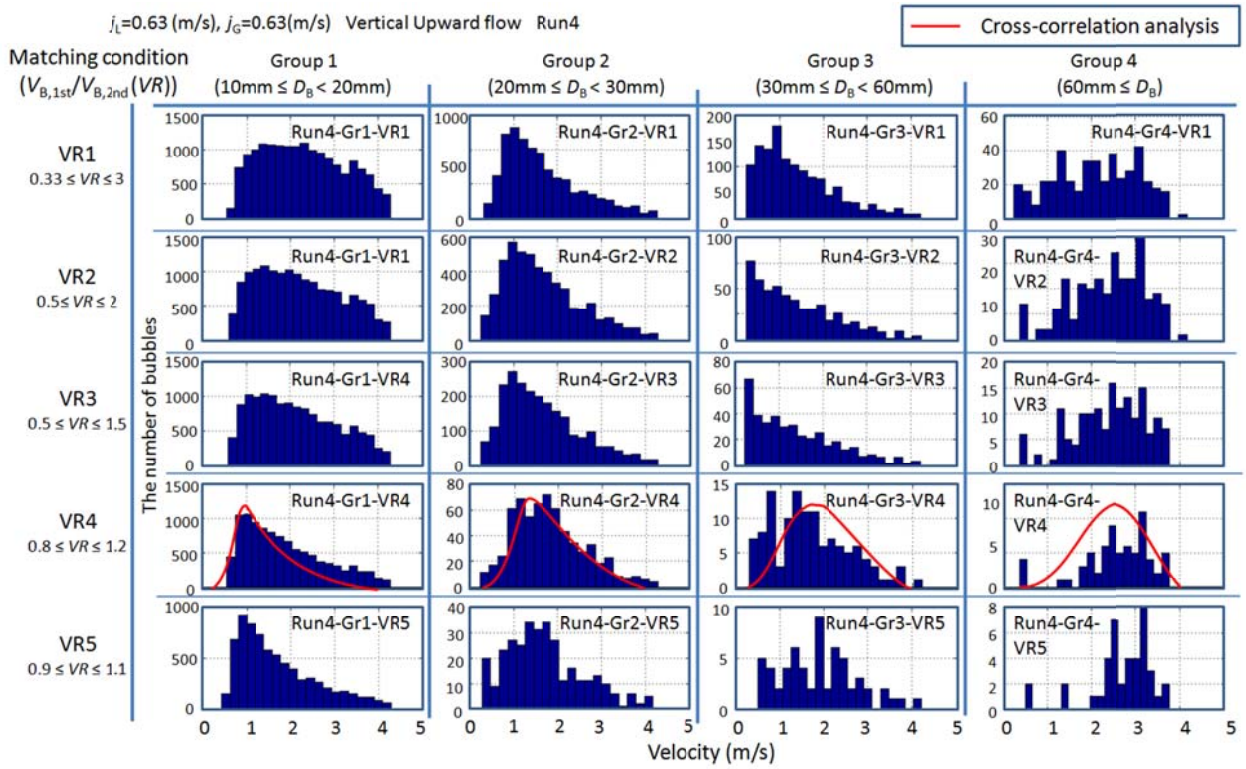

Fig. 5. Matching ratio versus $S_{B,1st}/S_{B,2nd}$.

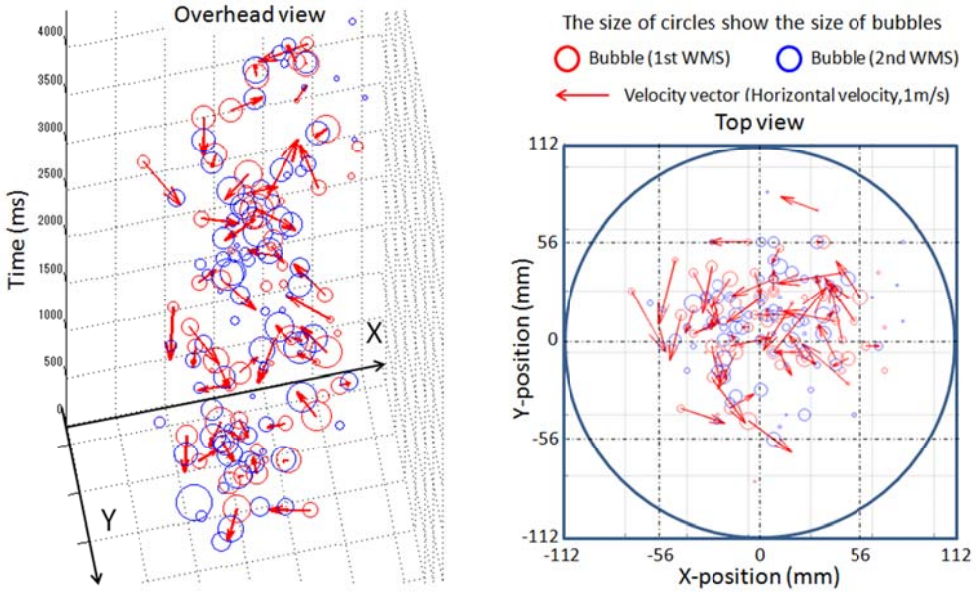

Fig.6. The bubble velocity of the swirl flow, j_G= 0.21 m/s, j_L=0.63 m/s using bubble tracking. Overhead view (left). Top view (right).

BUBBLE VELOCITY: Fig. 7 shows the bubble velocity distributions of the four bubble groups, with flow conditions of j_G=0.05, 0.63 m/s, j_L=0.63 m/s and straight flow. This result effectively shows how bubble velocity rises with increasing bubble size. When Run1-Gr1-VR4 is compared with Run4-Gr1-VR4, Run1-Gr1-VR4 shows shape profile, while conversely, Run4-Gr1-VR4 shows a broad profile. This is because, for high void fraction conditions, featuring a secondary flow with large bubbles, turbulence considerably intensifies. Via this bubble tracking method, the difference of the bubble velocity by bubble size can be evaluated.

A quantitative estimation of the multi-dimensional flow is performed using a circumference component ($|\boldsymbol{u}_{\mathbf{G,cmf}}|$) and a radial component ($|\boldsymbol{u}_{\mathbf{G,rad}}|$) of the phasic velocity. $|\boldsymbol{u}_{\mathbf{G,cmf}}|$ and $|\boldsymbol{u}_{\mathbf{G,rad}}|$ are given as Eqs. 6-7.

$$|\boldsymbol{u}_{\mathbf{G,cmf}}(x,y)| = |\boldsymbol{u}_{\mathbf{G,h}}(x,y)| \cos\theta_{x,y}\,, \tag{6}$$

$$|\boldsymbol{u}_{\mathbf{G,rad}}(x,y)| = |\boldsymbol{u}_{\mathbf{G,h}}(x,y)| \sin\theta_{x,y}\,, \tag{7}$$

Here, $|\boldsymbol{u}_{\mathbf{G,h}}|$ is a horizontal component of the phasic velocity and $\theta_{x,y}$ is the angle between the horizontal velocity and reference vectors. In the case of the $|\boldsymbol{u}_{\mathbf{G,cmf}}|$ estimation, the reference vector turns counterclockwise. When the bubbles rotate counterclockwise or clockwise, $|\boldsymbol{u}_{\mathbf{G,cmf}}|$ has a positive or negative value. In the case of the $|\boldsymbol{u}_{\mathbf{G,rad}}|$ estimation, when the bubbles flow toward the center or outside, $|\boldsymbol{u}_{\mathbf{G,rad}}|$ have positive or negative values respectively.

Figs. 8 and 9 show $|\boldsymbol{u}_{\mathbf{G,cmf}}|$ of all bubbles (left) and large bubbles (right). Figs. 8 and 9 show results of the vertical upward and swirl flows respectively. $|\boldsymbol{u}_{\mathbf{G,cmf}}|$ of the vertical upward flow show almost zero values, which means the vertical upward flow has no specific directionality in the circumferential direction. Conversely,$|\boldsymbol{u}_{\mathbf{G,cmf}}|$ of the swirl flow show almost positive values, which mean the large bubbles tend to move in the direction of the center.

Figs. 10 and 11 show $|\boldsymbol{u}_{\mathbf{G,rad}}|$ of all bubbles (left) and large bubbles (right). Figs. 10 and 11 show results of the vertical upward and swirl flows respectively. In the region of radial position at about 80 - 112 mm, $|\boldsymbol{u}_{\mathbf{G,rad}}|$ show positive values. These results mean bubbles tend to move in the direction of the center, and with large bubbles this tendency is epically strong.

Fig. 12 shows an example measurement of bubble interaction. Large bubbles arise intermittently and small bubbles are shown on the circumference of the large bubble. The small bubbles are classified into three groups, namely on the underside, upper side and outside of the large bubbles. Using this bubble tracking method and evaluation technique, the interaction between large and small bubbles can be evaluated.

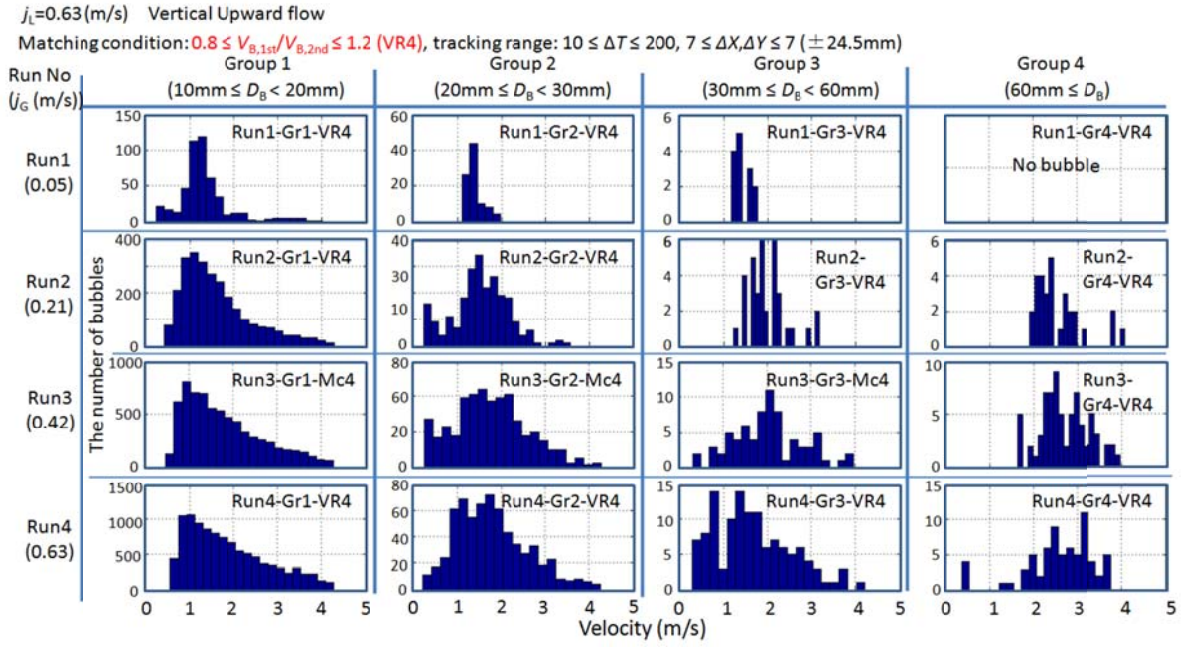

Fig. 7. Bubble velocity distributions of four bubble groups.

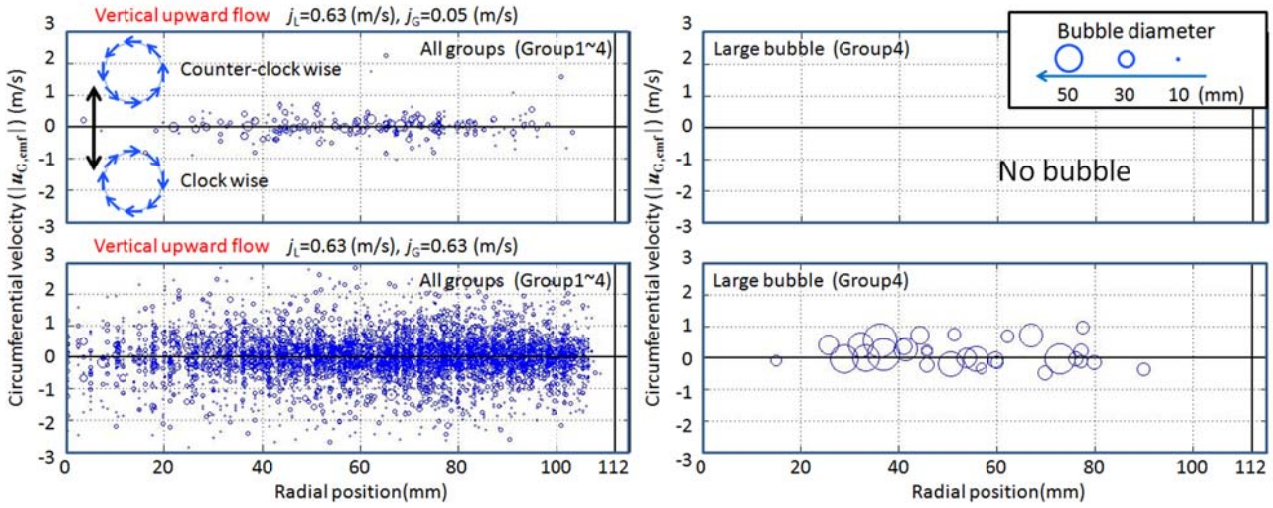

Fig. 8. Circumference (left) and radial (right) component of the bubble velocity in the vertical upward flow.

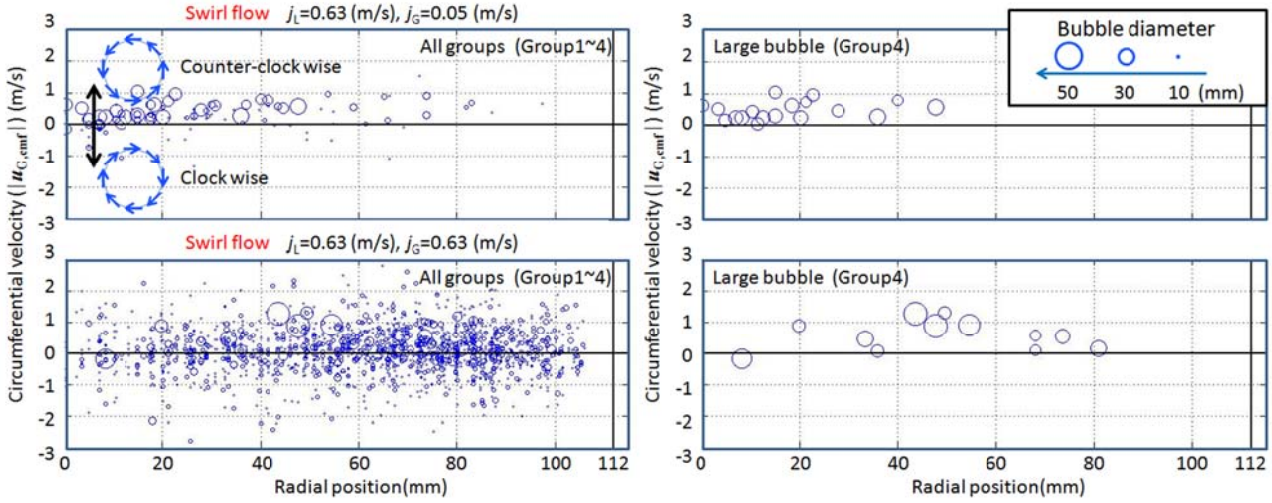

Fig. 9. Circumference (left) and radial (right) component of large bubble velocity in the vertical upward flow.

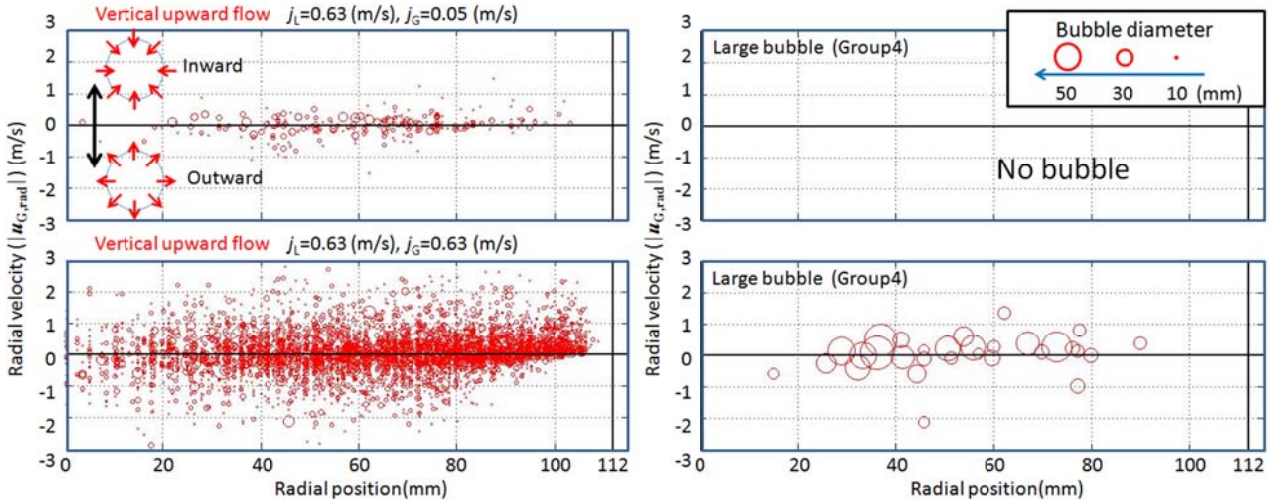

Fig. 10. Circumference (left) and radial (right) component of the bubble velocity in the swirl flow.

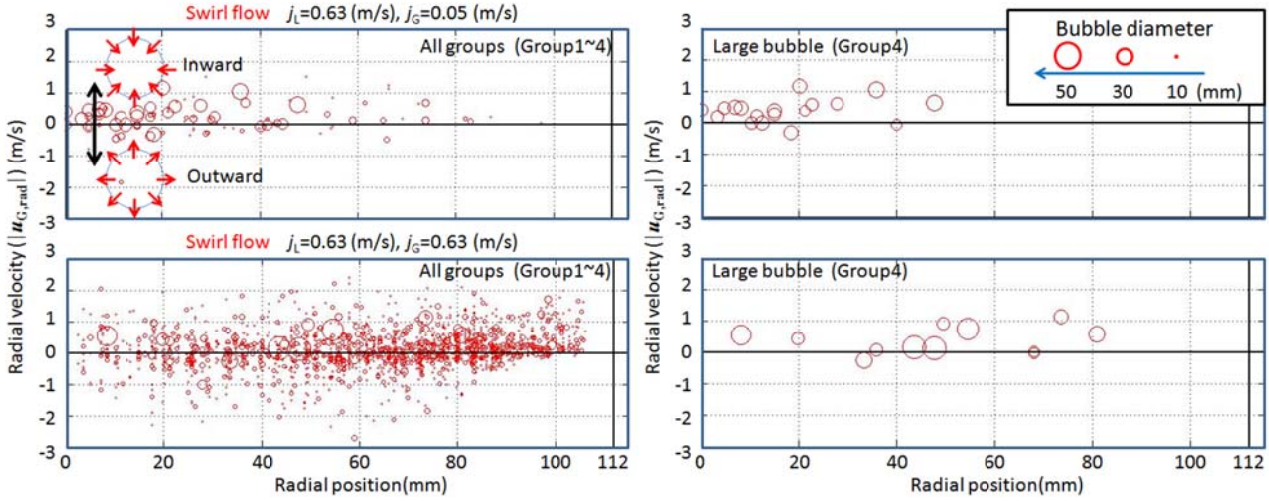

Fig. 11. Circumference (left) and radial (right) component of the large bubble velocity in the swirl flow.

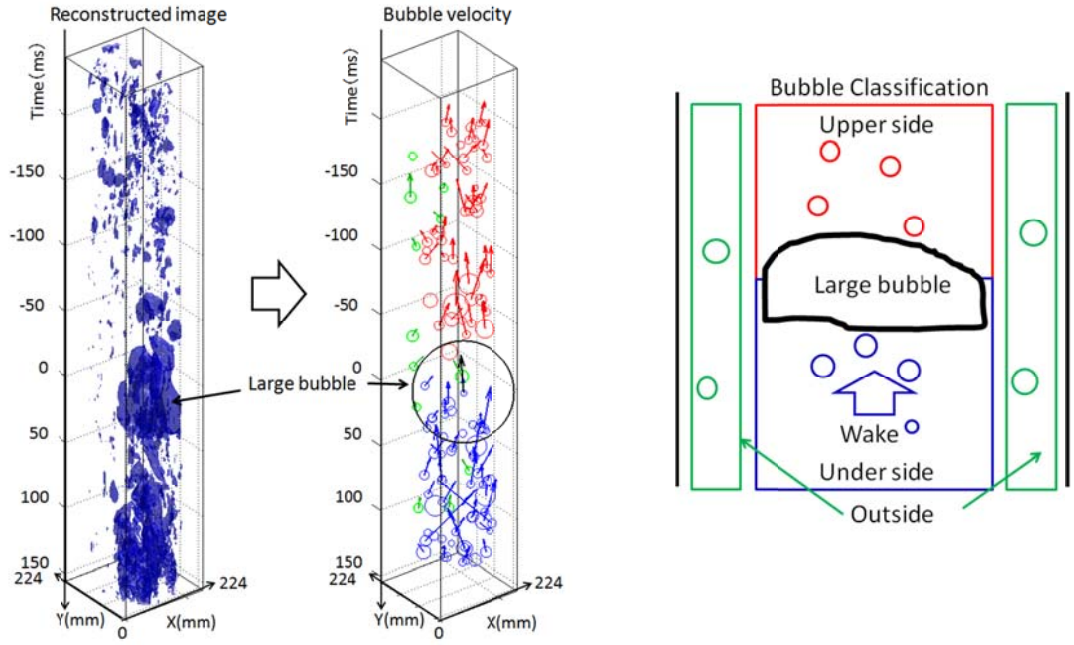

Fig. 12. Large bubbles which arise intermittently and small bubbles of the circumference of the large bubble.

CONCLUSIONS: We proposed an algorithm to estimate three-dimensional bubble velocity according to each WMS measurement locations. The three-dimensional phasic velocity is determined by the tracking bubble. The proposed algorithm first identifies each bubble in the WMS signals and subsequently seeks pairs of similar bubbles in two WMS data according to bubble size and location. The validity of this method is demonstrated for a swirl flow for which the proposed method can successfully visualize the structure. Using this bubble tracking method, the variation in bubble velocity due to bubble size and the interaction between large and small bubbles can be evaluated.

ACKNOWLEDGEMENTS: The authors would like to thank Professor H.-M. Prasser of ETH for his many helpful suggestions. Thanks also to Takeo Yoshioka of CERES Inc. and Yoshiyuki Shiratori, Hirokazu Kamata and Kunihiko Nishiyama of Electric Power Engineering Systems Co., Ltd., for their assistance in these experiments.

REFERENCES:

1. Aritomi, M. et al., 2000. Ultrasonic Doppler method for bubbly flow measurement. 5th Workshop on Meas. Tech. for Steady and Transient Multiphase Flows, Rossendorf, Germany.
2. Hogsett, S. T. et al., 1997. Local two-phase flow measurements using sensor techniques. Nucl. Eng. Des 175, p. 15-24.
3. Prasser, H. -M. et al., 1998. A new electrode-mesh tomograph for gas-liquid flows. Flow Meas. Instrum9, p. 111-119.
4. Weerin, W. et al., 2003. Intrusive Effect of Wire Mesh Tomography on Gas-liquid Flow Measurement. J. Nucl. Sci. Technol 40, p. 932.
5. Prasser, H. -M. et al., 2002. Fast wire-mesh sensors for gas-liquid flows-visualization with up to 10,000 frames per second. Proc. Int. Congress on Advance Nuclear Power Planes, Hollywood Florida, USA.
6. Richter, S. et al., 2002. Approach towards spatial phase reconstruction in transient churn flow using a wire mesh sensor. Int. J. Heat Mass Transfer 45, p. 1063.
7. Prasser, H. -M. et al., 2002. Evolution of the two-phase flow in a vertical tube–decomposition of gas fraction profiles according to bubble size classes using wire mesh sensors. Int. J. Therm. Sci 41, p. 17.
8. Manera, A. et al., 2006. Three-dimensional flow pattern visualization and bubble size distributions in stationary and transient upward flashing flow. Int. J. Multiphase Flow 32, p. 996.
9. Kanai, T. et al., 2011. Multi-dimensional Two-Phase Flow Measurements in a Large-Diameter Pipe Using a Wire-Mesh Sensor, Proc. ICONE 19, Osaka, Japan, CD-ROM, (2011)